Chain Dynamics in Elastomers As Investigated by Proton Multiple-Quantum NMR

Kay Saalwächter*,†

Institut für Makromolekulare Chemie, Universität Freiburg, Stefan-Meier-Str. 31, D-79104 Freiburg, Germany

Andreas Heuer

Institut für Physikalische Chemie, Universität Münster, Corrensstr. 30, D-48149 Münster, Germany

Received December 1, 2005; Revised Manuscript Received March 13, 2006

ABSTRACT: The influence of segmental and cooperative dynamics in elastomers on the time evolution in NMR experiments is considered using static proton multiple-quantum experiments. A novel experimental strategy as well as Monte Carlo simulations of a simple rotational diffusion model is used to investigate the applicability of the Andersen−Weiss approximation, upon which our analytical solutions are based. On the basis of temperature-dependent experiments, the validity of one of the most popular models used so far for the interpretation of NMR experiments is disproved. This model, which is based on slow rotational diffusion of a preaveraged residual coupling tensor, is refined by explicit consideration of the time scale of fast segmental processes which average the intrasegmental dipolar coupling toward a plateau value that is related to the chain order parameter associated with topological restrictions by chemical and physical cross-links. Models based on exponential or power-law loss of correlation are shown to provide physically reasonable representations of the data. As opposed to various earlier approaches, multiple-quantum NMR is unique in that it can be used to verify or falsify the different models. Data measured on permanently cross-linked systems are only weakly influenced by slow, cooperative processes, while reptation dynamics in corresponding linear-chain melts effectively prevents the observation of a well-defined order parameter.

1. Introduction

The variety of possibilities offered by NMR to assess elastomer microstructure is impressing.[1] A multitude of techniques can be used to estimate residual dipolar couplings or other anisotropic interactions and relate these to the density of cross-links or macroscopic properties of the network which depend on this quantity. Residual interactions arise from fast segmental fluctuations that are nonisotropic due to the existence of cross-links and other topological constraints[2,3] and are directly proportional to a dynamic order parameter S_b of the polymer backbone.

In a previous publication,[4] we have exemplified the advantages of a specific approach to multiple-quantum (MQ) NMR,[5−7] which is characterized by the possibility to normalize experimental DQ buildup data and thus remove any influences of relaxation processes on the DQ intensity.[8−10] This allows for the extraction of absolute values for residual dipolar couplings and thus order parameters and also to assess their distribution. While our previous work[4] was concerned with a quantitative interpretation of S_b in diene elastomers, we here focus on the influence of segmental dynamics on the observables.

The measurement of longitudinal relaxation times using for instance fast field-cycling instrumentation is among the most powerful approaches when the time scale of polymer dynamics is to be investigated[11] and has recently gained momentum in the field of elastomers.[12−14] The analysis of transverse relaxation behavior, in particular that of protons, is even more popular due to its simplicity. While an interpretation of such data in terms of quasi-static residual couplings gives reasonable results on chain order and thus elastomer microstructure,[15,16] the use of a dynamic model assuming a slowly fluctuating residual coupling is often favored.[17]

Transverse relaxation decays are notoriously featureless and influenced by a variety of factors, such that the use of multiparameter functions based on strong model assumptions may lead to severe fitting artifacts.[18,19] More specific experiments from which information on slow, cooperative processes was claimed to be extractable with better confidence have been introduced over the past decades. They are based on combinations of Hahn and solid echoes,[20,21] stimulated echoes,[12,22] or correlation loss in other dipolar refocusing experiments.[23] All these approaches are exclusively based on the assumption of rather slowly fluctuating residual couplings (down to the 0.1 ms scale), where segmental modes are always assumed to be too fast to exert an appreciable influence on the signal functions. In this regard, the only exception appears to be the transverse-relaxation theory of Brereton,[24] who explicitly considers fast Rouse modes. Its only experimental tests are however restricted to T_2 experiments on linear polymers.[25,26]

In this work, we present data which disprove the slow-motion assumption and show that fast segmental modes dominate transverse relaxation phenomena and thus NMR line width parameters in rubbers. On one hand, results from temperature-dependent experiments are in straightforward disagreement with the slow-motion *ansatz*, as the fitting results are simply unphysical. On the other hand, our MQ method generates two qualitatively different sets of data (a buildup curve and a decay curve), which depend differently on the relaxation processes and the residual coupling and provide a more reliable basis for fitting. This paper builds upon and extends the theoretical treatment presented in our earlier work,[10] which in turn has

* Corresponding author. E-mail: kay.saalwaechter@physik.uni-halle.de.
† New affiliation: Fachbereich Physik, Martin-Luther-Universität Halle-Wittenberg, Friedemann-Bach-Platz 6, D-06108 Halle, Germany.

10.1021/ma052567b CCC: $33.50 © 2006 American Chemical Society
Published on Web 04/08/2006

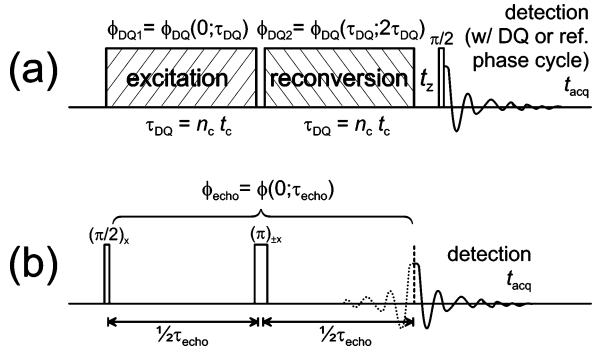

Figure 1. Timing schemes of multiple-quantum (a) and Hahn-echo (b) NMR experiments, along with a definition of phase factors which are acquired under a pulse sequence with a pure double-quantum Hamiltonian ($\phi_{DQ1,2}$) and during pure dipolar evolution over a Hahn-echo sequence (ϕ_{echo}).

basically generalized the treatment of the so-called "β function".[27]

Within the framework of the Andersen−Weiss (AW) approximation,[28] it is possible to test and evaluate different models for the loss or orientation correlation in rubbers. The applicability of the AW theory to polymer dynamics has been criticized,[29,24] and we here investigate the range of its validity by help of comparisons of MQ and simple transverse relaxation experiments as well as Monte Carlo simulations. We explore the properties of improved autocorrelation functions, discuss the results obtained from fits to experimental data, and conclude with a comparison of polymer networks and linear-chain melts, where large-scale chain diffusion (reptation) exerts a very specific influence on the measured data.[5]

2. Experimental Section

Samples. Natural rubber was kindly supplied by Malaysian Rubber (trade name CV 60). We have investigated two samples vulcanized with 0.4 and 3 phr sulfur (NR-A04 and NR-A3, respectively) as well as the linear, un-cross-linked precursor polymer (NR-lin). The M_n of the latter was estimated by membrane osmosis to be $(4 \pm 2) \times 10^5$ g/mol, with about 10 wt % insolubles that did not pass a 0.45 μm filter. Details on the preparation and characterization of the vulcanized rubbers can be found in ref 4. The calorimetric glass transition temperatures were determined by DSC: 208, 213, and 206 K, respectively.

NMR Spectroscopy. ^{1}H MQ and Hahn-echo experiments were performed following previously published procedures.[8,10,18,19] Schematic representations of the pulse sequences are given in Figure 1. The MQ experiment features a pulse sequence with a pure DQ average Hamiltonian[30] that has been modified slightly for better offset and pulse-imperfection compensation.[8] It excites all even quantum orders in a multispin system, and blocks of equal duration τ_{DQ} are applied to excite DQ (and higher-order MQ) coherences as well as to reconvert these into observable magnetization. A phase cycling scheme is applied to select a DQ-filtered (I_{DQ}) and a reference (I_{ref}) intensity. I_{DQ} subsumes signal from dipolar coupled segments and all $4n + 2$ quantum orders (as a result of the four-step selection phase cycle). I_{ref} contains contributions from all $4n$ quantum orders as well as dipolar-encoded longitudinal magnetization plus all signal from uncoupled, i.e., isotropically mobile components. The sum $I_{DQ} + I_{ref}$ comprises the full, dipolar-refocused magnetization of the sample and is subject to relaxation effects only. The corresponding analyzed quantity is

$$I_{\Sigma MQ} = I_{DQ} + I_{ref} - B \exp\{-2\tau_{DQ}/T_{2B}\} \tag{1}$$

where uncoupled contributions (sol, dangling ends) that appear as very slowly relaxing tails of I_{ref} are subtracted. The tails are most easily identified and fitted in a linearized representation of $\log\{I_{ref} - I_{DQ}\}$ vs τ_{DQ}, as explained in detail in ref 18. $I_{\Sigma MQ}$ and I_{echo} from Hahn-echo experiments are generally plotted on a scale set by $I(\tau{=}0) := 1$ (the intensity after a 90° pulse), such that the prefactor $A = 1 - B$ (contents of network chains) is easily identified as the starting value of the decay curves. A is generally used as a (fixed) prefactor in fits to all formulas given below for $I_{\Sigma MQ}$, I_{DQ}, and I_{echo}. The analysis of MQ and Hahn-echo data yielded comparable amounts of mobile components. Over the investigated temperature range, the amount of liquidlike components varied between less than 1% at low temperatures and 6% at high temperature for NR-A3, while it reached the 20% range for NR-A04 and NR-lin.

In permanently cross-linked systems, $I_{\Sigma MQ}$ can be used to *normalize* the DQ-filtered intensity, thereby removing the influence of relaxation effects on the data:

$$I_{nDQ} = I_{DQ}/I_{\Sigma MQ} \tag{2}$$

From about 50 K above the glass transition, the normalized DQ buildup data are then virtually temperature-independent over many tens of kelvin, providing evidence that effects of chain dynamics are largely absent in I_{nDQ} (see below). Using only intensities $I_{nDQ} \leq 0.45$, the normalized DQ buildup curves are analyzed with a buildup function based on a static second-moment approximation[10]

$$I_{nDQ}(D_{res}) = \frac{1}{2}\left(1 - \exp\left\{-\frac{8}{9}M_{2res}\tau_{DQ}^{\,2}\right\}\right) \tag{3}$$

The residual dipolar second moment is here given by its usual definition

$$M_{2res} = \frac{9}{20}D_{res}^{\,2} \tag{4}$$

Note that D_{res} is an *apparent* coupling constant and represents an average over many different internuclear pair couplings. Our previous work has shown that in unswollen elastomers the apparent distribution of couplings, thus deviations from the inverted-Gaussian form, are generally (and somewhat surprisingly) very weak.[8,31,19] Thus, models assuming a single, well-defined value for the residual coupling appear justified.

All experiments were performed on a Bruker minispec mq20 operating at 0.5 T (90° pulses of 1.9 μs length), which we have previously shown to produce fully quantitative results.[9] The experimental protocol is flexible in that $\tau_{DQ} = n_c t_c$ (see Figure 1) can be incremented by either using a fixed number of pulse sequence cycles n_c and varying the cycle time t_c or vice versa. On the minispec, the time-incremented two-cycle version ($n_c = 2$) is the most robust choice. Note that finite-pulse effects are taken into account by scaling τ_{DQ} by a duty-cycle-dependent scaling factor $a(\psi)$.[8] For simplicity, we do not explicitly consider this correction in the following. Our theoretical treatment given below assumes a continuous average DQ Hamiltonian, and the deviations which are expected when loss of correlation is evaluated for an actual sequence with finite, repetitive evolution intervals between pulses were treated in detail in an earlier paper[10] and are summarized in the Appendix. The basic finding is that the extracted fast correlation times may be overestimated by a factor of 1.5 when the much more compact continuous-limit formulas are used for fitting.

3. Results and Discussion

The temperature dependence of I_{DQ} and $I_{\Sigma MQ}$ as well as the absence of relaxation effects in I_{nDQ} is demonstrated in Figure 2. Beyond its use in normalizing buildup data, $I_{\Sigma MQ}$ is a valuable source of information on chain dynamics. Its decay is completely free of the dipolar dephasing effects which dominate the decay of Hahn echoes, and the salient advantage of the MQ method is that simultaneous fits to I_{DQ} and $I_{\Sigma MQ}$ allow us to test and verify or falsify different models used to describe the influence of chain dynamics.

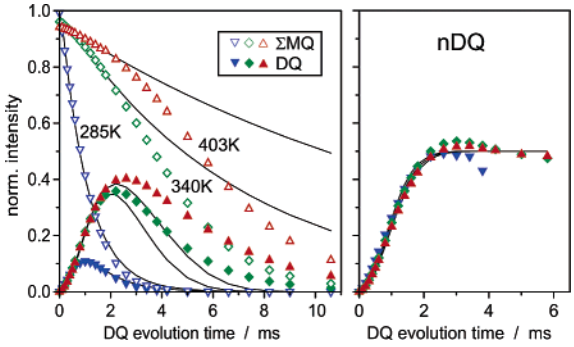

Figure 2. Experimental data from MQ experiments on NR-A3 over a wide temperature range. The temperature interval is limited by the increasingly strong relaxation effects at low T (which preclude reliable fitting) and sample decomposition at high T. The solid lines on the left are independent fits to the slow-motion model and are discussed further in the text. On the right, the lines are fits to eq 3.

In the following, we first outline the theory used to analyze the experiments, present new experimental and theoretical evidence on the validity of the Andersen−Weiss *ansatz* that is central to the theory, and discuss general features of MQ data calculated on the basis of different models for chain dynamics. We discuss the results obtained from fitting the different theoretical model functions to actual data and conclude with a comparison of data obtained for permanently cross-linked networks on one hand and corresponding linear melts on the other hand.

A. The Andersen−Weiss Approximation and Its Validity. The following treatment is formally equivalent to the theory presented by Ball, Callaghan, and Samulski (BCS) for the description of a specific solid-echo-based experiment termed the β echo.[27] In a previous publication,[10] we have shown that the BCS treatment can directly be used for the description of an MQ experiment, the difference only being a scaling factor related to evolution under a pure DQ Hamiltonian

$$\bar{H}_{DQ} = -\frac{a(\psi)}{2}\sum_{i<j} D_{eff}^{(ij)} P_2(\cos\beta_{ij})(\hat{I}_+^{(i)}\hat{I}_+^{(j)} + \hat{I}_-^{(i)}\hat{I}_-^{(j)}) \quad (5)$$

as opposed to free dipolar evolution.

The network contributions to the DQ-filtered and reference intensities are generally dominated by spin-pair contributions, i.e., pure DQ coherences and dipolar-encoded longitudinal magnetization (LM), respectively.[7] Analytical representations for I_{DQ} and $I_{\Sigma MQ}$ are therefore easily derived as

$$I_{DQ} = \langle \sin\phi_{DQ1} \sin\phi_{DQ2}\rangle \quad (6)$$

$$I_{\Sigma MQ} = \langle \sin\phi_{DQ1} \sin\phi_{DQ2}\rangle + \langle \cos\phi_{DQ1} \cos\phi_{DQ2}\rangle \quad (7)$$

Phase factors are calculated as integrals over the second Legendre polynomial of the fluctuating polar orientation β_t of the effective interaction tensor

$$\phi_{DQ} = D_{eff}\int_{\tau_a}^{\tau_b} P_2(\cos\beta_t)\, dt \quad (8)$$

where the time intervals are chosen according to the pulse sequence (see Figure 1a). A corresponding treatment of a simple Hahn (not solid!) echo experiment yields the dipolar-dephasing function

$$I_{echo} = \langle \cos\phi_{echo}\rangle \quad (9)$$

where the phase factor is now given by

$$\phi_{echo} = \frac{3}{2} D_{eff}\int_0^{\tau_{echo}} P_2(\cos\beta_t)\, dt \quad (10)$$

Note the usual prefactor of $^3/_2$ which arises for spin evolution under homonuclear dipolar couplings (strong coupling limit).

When the interaction frequency distribution is assumed to be Gaussian, the classic arguments of Andersen and Weiss can be used to rearrange eqs 6−8 to yield

$$I_{DQ} = \sinh(\langle\phi_{DQ1}\phi_{DQ2}\rangle)\exp(-\langle\phi_{DQ1}{}^2\rangle) \quad (11)$$

$$I_{\Sigma MQ} = \exp(\langle\phi_{DQ1}\phi_{DQ2}\rangle)\exp(-\langle\phi_{DQ1}{}^2\rangle) \quad (12)$$

$$I_{echo} = \exp\left(-\frac{1}{2}\langle\phi_{echo}{}^2\rangle\right) \quad (13)$$

Note that $\langle\phi_{DQ2}{}^2\rangle = \langle\phi_{DQ1}{}^2\rangle$ because the averages are uncorrelated. It should be emphasized that the Gaussian approximation, corresponding to the second-order cumulant expansion, is valid over the whole range from the static case, where the second moment of the frequency distribution is associated with the width of the corresponding Pake pattern, to the fast limit of an isotropic thermal random process, where all possible orientations are successively sampled by a single segment. Limitations, to be discussed below, must be expected in the slow-motion limit, where only the initial part of a time-domain signal associated with a Pake spectrum has a Gaussian form. In this limit, care must also be taken when a preferential macroscopic orientation (e.g., in a strained rubber) is present and the isotropic powder distribution is modified.

Equations 11−13 can be used to establish an *experimental* test of the Gaussian approximation, which is completely independent of the choice of the autocorrelation function (henceforth ACF) used to evaluate the averages over the phase factors (see below). This becomes possible because the phase factors ϕ_{DQ} and ϕ_{echo}, given by eqs 8 and 10, respectively, differ only in the well-established prefactor of $^3/_2$ constituting the only qualitative difference between formulas for spin-pair evolution under an average DQ and a pure dipolar Hamitonian (note again that the duty-cycle-dependent scaling factor of the DQ average Hamiltonian, eq (5), is always absorbed into the time axis). A suitable combination of eqs 11 and 12 can be used to eliminate the mixed phase factor $\langle\phi_{DQ1}\phi_{DQ2}\rangle$. Equating $\langle\phi_{DQ1}{}^2\rangle$ and $^4/_9\langle\phi_{echo}{}^2\rangle$ yields

$$I_{echo} = \left[I_{\Sigma MQ}{}^2\left(1 - \frac{2I_{DQ}}{I_{\Sigma MQ}}\right)\right]^{9/16} \quad (14)$$

This identity is put to a test in Figure 3. It is seen that experimental and "theoretical" Hahn-echo decays are in convincing agreement over the whole investigated temperature range. Deviations occur and must of course be expected at longer times, where, as mentioned above, a spin-pair dipolar echo decay associated with a Pake spectrum starts to deviate from a Gaussian function. This occurs at an evolution time (τ_{DQ}) of about 1.8 ms, during which the *normalized* DQ intensity for the same sample has reached about 0.45. This is in fact the limit up to which we have observed good correspondence between a Gaussian-shaped quasi-static DQ buildup, eq 3, and experimental as well as simulated data for spin pairs and multispin systems.[4,8] Using eq 3, the validity limit for a permanent network is calculated as

$$\tau_{DQ}^{max} = 2.4/D_{res} \quad (15)$$

CDV

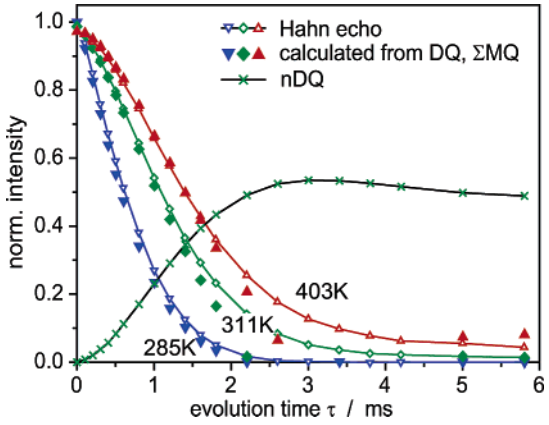

Figure 3. Experimental Hahn-echo decay curves of NR-A3 (open symbols), compared to "theoretical" intensities (closed symbols) which were calculated from experimental MQ data measured at the same temperatures using eq 14. An experimental normalized DQ buildup curve of the same sample is shown for comparison.

where D_{res} is in rad/s (i.e., it includes a factor of 2π). In our previous work,[10] we have already pointed out that the presented theory based on dominant pair interactions cannot be expected to hold at longer times, where multispin effects come into play, and we have tentatively proposed to fit only the initial 30% of the decay of $I_{\Sigma MQ}$. Equation 15 constitutes a more rigorously defined limit, beyond which the AW approximation cannot be expected to hold. In many earlier works, in particular those on Hahn-echo experiments, fits were performed over the whole time range. This of course leads to systematic errors and to potentially serious fitting artifacts when the long-time shapes of the curves deviate from the AW prediction.

The second step of the AW treatment consists of evaluating the time and ensemble averages of the phase factors in eqs 11−13 in terms of an orientation ACF $C(t)$ of the effective dipolar tensor

$$C(|t_a - t_b|) = \langle P_2(\cos\beta_{t_a})\, P_2(\cos\beta_{t_b})\rangle \qquad (16)$$

which describes the loss of "orientational memory" of the polar orientation of the fluctuating effective intrasegmental dipolar tensor. For example, for the mixed product of DQ phases, the average becomes

$$\langle\phi_{DQ1}\phi_{DQ2}\rangle = \frac{4}{9}M_{2eff}\int_0^{\tau_{DQ}}\int_{\tau_{DQ}}^{2\tau_{DQ}} C(|t_a - t_b|)\, dt_a\, dt_b \qquad (17)$$

where the powder average simply leads to a factor of $^1/_5$ that is absorbed into the definition of M_{2eff} (see below).

A typical ACF expected for network chain segments is depicted in Figure 4. The first, most prominent decay corresponds to fast segmental fluctuations that are ultimately constrained by topological restrictions (entanglements) and the permanent cross-links. These motions may be associated with local Rouse modes. The plateau value is given by the square of the dynamic residual order parameter of the polymer backbone, S_b. Further loss of correlation is commonly attributed to slow cooperative dynamics of the cross-links and is assumed to be orders of magnitude slower than the segmental process. As indicated above, most earlier approaches assume that the segmental modes are too fast to exert an appreciable influence on transverse relaxation phenomena. For the slow process,

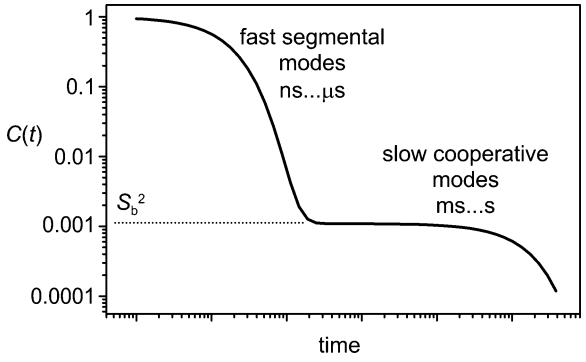

Figure 4. Schematic representation of an orientation ACF for network chain segments far above T_g.

isotropic rotational diffusion is a popular model, as is described by a simple exponential ACF

$$C(t) = S_b^{\,2}\exp\{-t/\tau_s\} \qquad (18)$$

Below, we will also test whether a simple exponential decay might also be able to model the fast segmental process

$$C(t) = (1 - S_b^{\,2})\exp\{-t/\tau_f\} + S_b^{\,2} \qquad (19)$$

A third and seemingly more realistic *ansatz* is to combine the above cases

$$C(t) = (1 - S_b^{\,2})\exp\{-t/\tau_f\} + S_b^{\,2}\exp\{-t/\tau_s\} \qquad (20)$$

which is plotted in Figure 4.

The weak residual degree of anisotropy, as described by S_b^2, is proportional to M_{2res}, eq 4, and S_b itself is given by

$$S_b = D_{res}\frac{k}{D_{stat}} \qquad (21)$$

The effective second moment, to be used in calculations such as eq 17, is then given by

$$M_{2eff} = \frac{9}{20}\left(\frac{D_{stat}}{k}\right)^2 \qquad (22)$$

A comparison of eqs 4, 21, and 22 demonstrates that $M_{2res} = S_b^2 M_{2eff}$.

We define $C(t)$ such that the case of $C(0) = 1$ is associated with a fully extended network chain, where an intrasegmental static-limit apparent coupling constant D_{stat}/k, or the related second moment M_{2eff}, is assumed to comprise an average over even faster intrasegmental local conformational rearrangements. These reduce the different intramonomer dipolar tensors to a uniaxially averaged quantity that is associated with the effective orientation of the statistical (Kuhn) segment. The assumption of uniaxial symmetry is reasonable and greatly simplifies the treatment as well as a comparison with theory, as discussed in much detail in ref 4. On the basis of extensive simulations, we have found $D_{stat}/k = 2\pi \times 6.3$ rad/s for natural rubber. As $D_{stat}/2\pi$ is typically on the order of 20 kHz for protons coupled to the same carbon, k is in the range 0.25−0.5 (0.5 would be the result of simple rotational averaging with the pair vector perpendicular to the symmetry axis, but this should not be taken too literally, as many different pairs are involved). D_{stat}/k is of course a model-dependent quantity, and in particular the absolute value results for the time scale of fast segmental modes depend on this choice.

B. Monte Carlo Simulations. We conclude our assessment of the AW approximation with a test that is based on Monte Carlo simulations of a rotational reorientation process. Note that this simulation does not claim to describe real network behavior but is rather meant to assess the validity of AW for the model tested. We have simulated rotational diffusion with fixed jump angles α (= grid spacing) ranging between 4.7° and 33.1° and recorded I_{DQ}, $I_{\Sigma MQ} = \langle\cos(\phi_{DQ1} - \phi_{DQ2})\rangle$ (dipolar echo, no dephasing), and

$$I_{\Delta MQ} = I_{\Sigma MQ} - 2I_{DQ} = \langle\cos(\phi_{DQ1} + \phi_{DQ2})\rangle \qquad (23)$$

Apart from a scaling of the time axis and the interaction strength, this latter quantity is formally equivalent to I_{echo} and reflects simple dipolar dephasing with $\phi_{DQ1} + \phi_{DQ2}$ as the acquired phase. For the same set of data we have calculated the phase factors and evaluated eqs 6 and 7 explicitly and also calculated the terms entering the AW approximations, eqs 11 and 12, for a comparison.

We have generated 100 000 independent trajectories to obtain a good signal-to-noise ratio. To mimic a stationary process with a finite order parameter S_b^2 as characterized by eq 19, our procedure was as follows: (i) Choose a random orientation Ω_0. (ii) For any orientation Ω define an energy functional $H(\Omega_0,\Omega) = -s\cos(\varphi(\Omega_0,\Omega))$, where $\varphi(\Omega_0,\Omega)$ describes the angle between the orientations Ω_0 and Ω. The use of P_1 rather than P_2 as energy functional models the realistic case that a network chain segment will rather be oriented along rather than in opposition to the end-to-end vector (yet the qualitative results do not depend on this choice). s is a constant which determines the final value of S_b^2 ($s = 0$ corresponds to $S_b = 0$ and, e.g., $s = 2.5$ corresponds to $S_b \approx 0.27$). (iii) Choose an initial orientation Ω_1 which corresponds to an equilibrium orientation according to the energy functional H. Its probability is thus determined by the "Boltzmann factor" $\exp\{-H(\Omega_0,\Omega_1)\}$. (iv) To obtain a time series, one generates a sequence of randomly chosen new orientations (again using a jump angle α) using an exponentially distributed waiting time with average τ_r. According to the standard Metropolis criterion, the new orientation is only accepted if either the difference ΔH between the new value and the old value of H is negative or, otherwise, a random number between 0 and 1 is smaller than $\exp(-\Delta H)$. This procedure guarantees that the distribution of orientations, generated in this way, is proportional to the "Boltzmann factor" $\exp\{-H(\Omega_0,\Omega_1)\}$. Isotropic rotational diffusion according to eq 18, with a decay time denoted as τ_s, is straightforwardly obtained using $s = 0$. Indeed, independently of the jump angle, the rotational dynamics generated in these ways was found to closely follow eqs 18 and 19.

The correlation functions are characterized by two dimensionless parameters, namely $M_{2res/eff}\tau_{s/f}^2$ and S_b, which were varied to check the behavior of signal functions in the slow- and fast-motion regimes. In Figure 5a, an isotropic model (corresponding to what is often used for "slow" motions of the residual tensor) is tested over a range that covers the transition from the quasi-static regime to fast motions that almost fully average M_{2res}. Note that upon approaching the fast limit $I_{\Sigma MQ}$ exhibits a transition from a Gaussian-type (parabolic) to an exponential decay (which is somewhat obscured by the semilog representation).

Within the fitting limits specified above, $I_{\Sigma MQ}$ is seen to perfectly follow the AW prediction, while some deviations occur for I_{DQ} toward larger τ_s. For the fast-motion model with a plateau given by S_b shown in (b), $I_{\Sigma MQ}$ is similarly well predicted by AW, and the same type of deviation occurs for I_{DQ}, but now

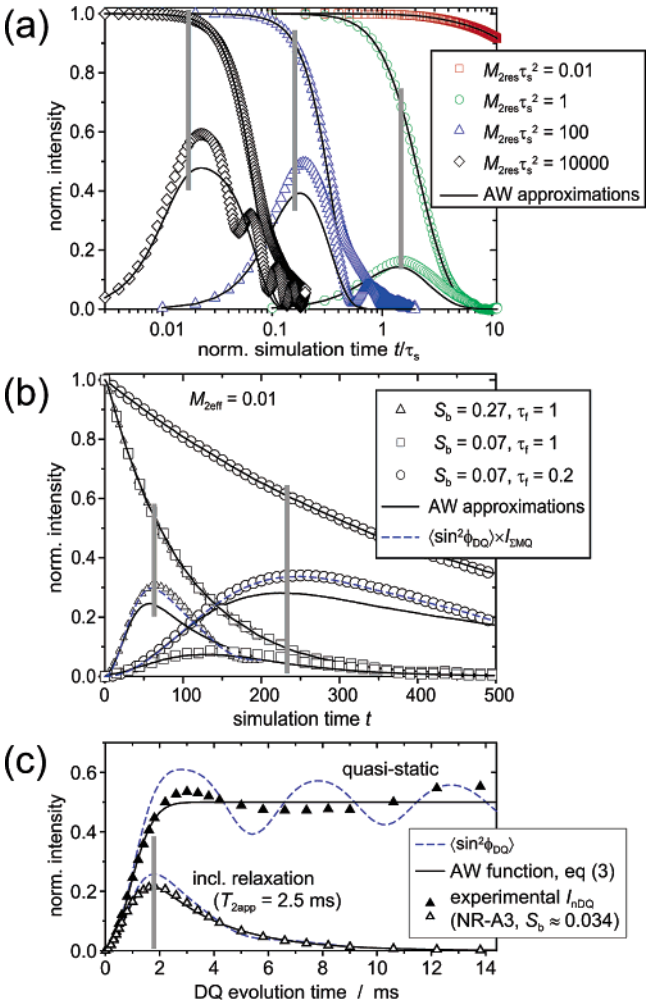

Figure 5. Comparison of explicit Monte Carlo simulations of DQ buildup and ΣMQ decay, eqs 6 and 7, with their AW approximations, eqs 11 and 12, for an isotropic rotational diffusion model (a) and the fast-motion model with a plateau (b). Symbols are from the explicit simulations, and lines are the corresponding AW approximations. In (b), the data are also compared with explicit quasi-static powder-averaged solutions for I_{DQ} damped by the simulated $I_{\Sigma MQ}$ as relaxation term (dashed lines). In (c), the difference between an actual powder average (dashed), the second-moment approximation (solid line), and typical experimental data (symbols) for I_{nDQ} is demonstrated for the quasi-static case and in the presence of exponential relaxation. The fitting limits according to eq 15 are indicated by vertical bars in all graphs.

for smaller τ_f or larger S_b. Generally, the deviations are prominent when I_{DQ} rises more quickly than $I_{\Sigma MQ}$ decays.

In all cases, this disagreement is due to the fact that the AW treatment assumes a Gaussian distribution of frequencies, while the starting point is of course a spin-pair single-interaction treatment, where the powder average over $P_2(\cos\beta)$ corresponds to a Pake-like frequency spectrum rather than a Gaussian. The oscillations in Figure 5a are simply the result of the powder average in eq 6, and they are observable because the correlation loss is comparably weak on their time scale. This is further demonstrated in (b), where quasi-static powder solutions damped by $I_{\Sigma MQ}$ as relaxation term (dashed lines) model the explicitly simulated data very well. We checked that additional consideration of higher-order terms of the cumulant expansion (the AW approximation corresponding to the second-order term) yields only a minor improvement. This has to be expected because within the framework of cumulant expansions one cannot obtain negative values.

Reassuringly, two-parameter fits of the theoretical functions introduced in the next section to the explicit simulation data reproduced the couplings within 10% and the correlation times within 40%, which is still good, as experimentally we will see that the latter varies over orders of magnitude. The failure of AW to describe the powder distribution is therefore not serious. As additional confirmation, Figure 5c shows that actual experimental data for I_{nDQ}, which is free of relaxation effects and can thus be analyzed in the quasi-static limit, is actually better described by the second-moment formula, eq 3, than by the powder solution. Fits to experimental data might therefore be even better justified in this regard.

We have previously shown that the damping of the oscillations is primarily due to couplings between multiple protons within the monomeric units,[4,8] and this phenomenology was of course the initial motivation for the AW approximation.[28] We believe that the apparent failure of AW as observed by Brereton[24] is due to his use of Gaussian statistics for the end-to-end vector that should lead to a broad gamma distribution of couplings. This distribution is, however, never observed in dry networks, as discussed in more detail in refs 4 and 32.

In what follows we present a different approximation for $I_{\Sigma MQ}$ (thus also I_{echo}) that might turn out to be useful in the context of ^{2}H NMR experiments, where multiple couplings are of no concern. For this purpose we first introduce an alternative microscopic realization which also gives rise to the same rotational correlation function eq 19, which will turn out to be the experimentally relevant one. Again we consider a jump process with an exponentially distributed waiting time τ_f. Now with probability $1 - S_b$ the jumper selects a randomly chosen orientation and with probability S_b a fixed orientation Ω (with NMR frequency $\omega_\Omega \sim M_{eff}^{1/2}$). Different jumpers are characterized by different fixed orientations Ω. Formally, the function $I_{\Delta MQ}(t)$ can be written as $\langle \exp(i(\sum \omega_i \Delta t_i)) \rangle$, where the sum in the exponent contains the contributions of the different orientations, taken by the jumper. On average, a fraction of S_b frequencies are identical to ω_Ω, whereas the remaining frequencies are randomly distributed. In the limit $t \gg \tau_f$, where fluctuations of these fractions can be neglected, one can write $I_{\Delta MQ}(t) \approx \langle \exp(iS_b\omega_\Omega t)\rangle_\Omega I'_{\Delta MQ}((1 - S_b)t)$, where $I'_{\Delta MQ}$ corresponds to the simple random-jump case with no orientational correlation. Approximating this function by the AW formula in the limit $t \gg \tau_f$, one finally ends up with

$$I_{\Delta MQ}(t) \approx \langle \exp(iS_b\omega_\Omega t)\rangle_\Omega \exp\left(-\frac{8}{9}M_{2eff}\tau_f t(1 - S_b)\right) \quad (24)$$

The first factor corresponds to the quasi-static dephasing function. It depends on the dimensionless parameter $t_{eff} = S_b M_{2eff}^{1/2} t$. Thus, one can first obtain the quasi-static FID via straightforward simulations and then evaluate this function for any value of M_{2eff}, t, and S_b. The above result justifies the use of an additional exponential term in fits to T_2 relaxation data,[17] but we emphasize again that a reliable multiparameter fit to a single data set is hardly possible.[19]

The above estimation is compared with explicit simulation results and AW approximations in Figure 6. One can clearly see that now a very good agreement with $I_{\Delta MQ}(t)$ is achieved for $t \gg \tau_f$. In contrast, for smaller times the AW approximation is superior. We also show $I_{DQ} = (1/2)(I_{\Sigma MQ} - I_{\Delta MQ})$, as obtained from our simulations. On one hand, it is compared with the AW approximation and, on the other hand, by using eq 24 rather than the AW approximation for $I_{\Delta MQ}$. Again, we find that the agreement for $t \gg \tau_f$ is very good for the latter estimation.

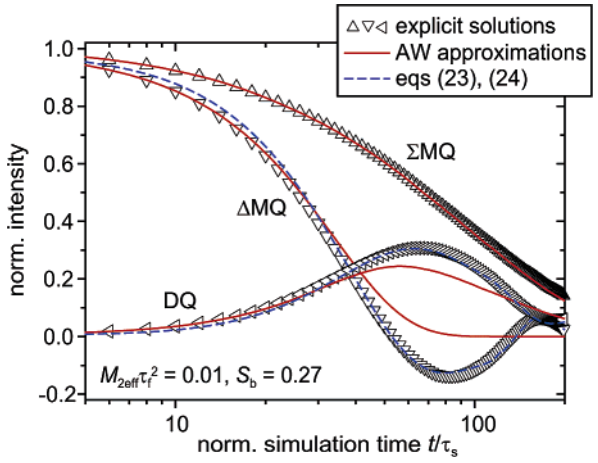

Figure 6. Comparison of $I_{\Sigma MQ}$, $I_{\Delta MQ}$, and I_{DQ} with the respective AW approximations, using eq 24 as an approximation for $I_{\Sigma MQ}$ and eq 23 to also obtain I_{DQ}.

In summary, we may conclude that, within the relevant fitting limit and our rotational diffusion model, the AW approximation works extremely well in all dynamic regimes for $I_{\Sigma MQ}$, whereas for I_{DQ} small deviations occur that are not very relevant when a simultaneous fitting is performed and are further not expected to play a significant role for actual experimental data on proton systems. For the analysis of ^{2}H transverse dephasing or DQ data, a significant improvement can be reached for $M_{2eff}\tau_f^2 \ll S_b^2 \ll 1$ when using eq 24 for the estimation of $I_{\Delta MQ}$, where very nice agreement is found even for long evolution times.

C. Testing Different ACFs. Slow-Motion Model. The common model based on negligible relaxation effects of fast-limit segmental motions and dominant slow motions of the residual dipolar tensor, as expressed by the ACF given by eq 18, leads to results for the signal functions, eqs 11−13, that were (up to a factor of $(^3/_2)^2$) already presented in refs 10 and 27

$$I_{DQ} = \exp\left\{-\frac{8}{9}S_b^2 M_{2eff}\tau_s^2\left(e^{-\tau_{DQ}/\tau_s} + \frac{\tau_{DQ}}{\tau_s} - 1\right)\right\} \sinh\left\{\frac{4}{9}S_b^2 M_{2eff}\tau_s^2(e^{-2\tau_{DQ}/\tau_s} - 2e^{-\tau_{DQ}/\tau_s} + 1)\right\} \quad (25)$$

$$I_{\Sigma MQ} = \exp\left\{-\frac{4}{9}S_b^2 M_{2eff}\tau_s^2\left(4e^{-\tau_{DQ}/\tau_s} - e^{-2\tau_{DQ}/\tau_s} + \frac{2\tau_{DQ}}{\tau_s} - 3\right)\right\} \quad (26)$$

$$I_{echo} = \exp\left\{-S_b^2 M_{2eff}\tau_s^2\left(e^{-\tau_{echo}/\tau_s} + \frac{\tau_{echo}}{\tau_s} - 1\right)\right\} \quad (27)$$

Note that the quasi-static buildup function, eq 3, follows directly from eq 25 in the limit $\tau_s \to \infty$. The relation for I_{echo} is well-known and has often been used in T_2 relaxometry.[17]

Equations 25 and 26 were used to *independently* fit the experimental I_{DQ} and $I_{\Sigma MQ}$ for the sample NR-A3 presented in Figure 2, left panel. Fits to I_{nDQ} on the right using eq 3 gave residual couplings around 205 Hz, which define the fitting limit $\tau_{DQ} \leq 1.8$ ms via eq 15. The results are compiled in Table 1 and are plotted in Figure 7.

The order parameters shown in Figure 7a as well as the correlation times in Figure 7b depend on the choice of M_{2eff}. According to eq 22, $M_{2eff} = 7.05 \times 10^8$ rad^2/s^2 when we use our previous result for $D_{stat}/k = 2\pi \times 6300$ rad/s for natural rubber.[4] While the S_b from I_{nDQ} and I_{DQ} are compatible over

CDV

Table 1. Results of the Various Fits to Temperature-Dependent MQ Experiments Performed on the Sample NR-A3[a]

	norm (nDQ)	slow-motion ACF (DQ)		slow-motion ACF (ΣMQ)		fast-motion ACF (DQ & ΣMQ simult)		combined ACF (DQ & ΣMQ simult)			power-law ACF (DQ & ΣMQ simult)		
temp/K	S_b	S_b	τ_s/ms	S_b	τ_s/ms	S_b	τ_f/μs	S_b	τ_f/μs	τ_s/ms	S_b	τ_0/ns	κ
267	0.0419	0.189	0.06	>1[b]	0.0052	0.0497	5.30	0.0548	5.2	2.38	0.0473	2400	1.71
285	0.0341	0.0513	0.56	0.174	0.051	0.0362	1.42	0.0411	1.2	3.11	0.0290	120	0.91
303	0.0338	0.0373	1.89	0.0833	0.098	0.0344	0.60	0.0360	0.51	9.40	0.033	20	0.78
321	0.0335	0.0341	4.45	0.0505	0.145	0.0340	0.31	0.0348	0.24	15.7	0.0313	3.7	0.71
340	0.0329	0.0330	8.13	0.0348	0.190	0.0332	0.18	0.0338	0.14	25.2	0.0313	0.76	0.65
349	0.0330	0.0337	8.57	0.0313	0.170	0.0329	0.13	0.0337	0.10	20.7	0.0311	0.29	0.62
367	0.0322	0.0321	13.7	0.0279	0.200	0.0325	0.12	0.0327	0.11	74.0	0.0310	0.23	(0.62)
385	0.0319	0.0321	16.0	0.0235	0.210	0.0321	0.09	0.0324	0.07	43.6	0.0310	0.11	0.61
403	0.0311	0.0316	15.7	0.0248	0.163	0.0313	0.08	0.0316	0.06	50.0	0.0303	0.09	(0.60)
421	0.0267	0.0300	19.0	0.0219	0.215	0.0267	0.08	0.0268	0.08	(100)	0.0254	0.06	0.58

[a] Parentheses indicate suitably chosen values that were held constant due to fitting instabilities. [b] Unphysical best-fit result.

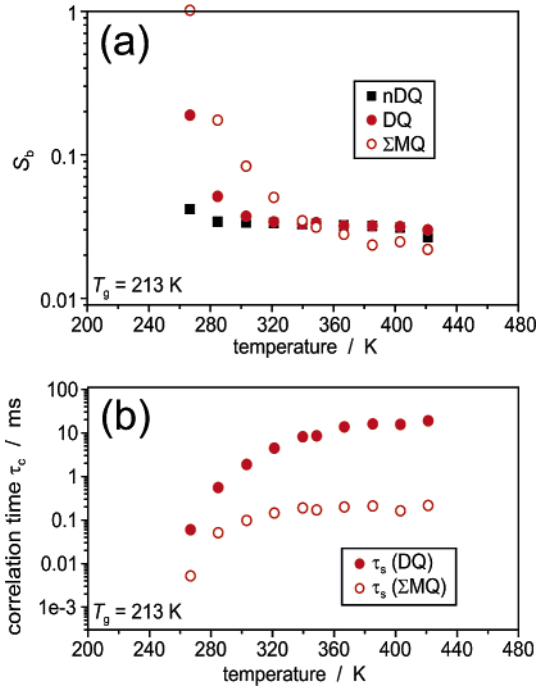

Figure 7. Order parameters (a) and slow correlation times (b), obtained by fits to the experimental data for NR-A3 shown in Figure 2, using eq 3 as well as eqs 25 and 26 for the slow-motion model. The results in (b) are plainly unphysical, proving the inadequacy of this model.

most of the temperature range, significantly different and strongly temperature-dependent values are obtained from fits to $I_{\Sigma MQ}$. This finding alone shows that the slow-motion model is not applicable, as the same results should be obtained from the two sets of data. In our previous work,[10] we have compared residual couplings obtained for PDMS networks at room temperature, where fits to $I_{\Sigma MQ}$ gave significantly smaller values for S_b than fits to I_{nDQ}. This was at that time interpreted as an indication for restricted (rather than free) rotational diffusion of the residual dipolar tensor. Here we see that this interpretation cannot hold and that the finding is related to the fact that room temperature for PDMS is about 160 K above T_g, where also here the S_b determined from $I_{\Sigma MQ}$ falls below the correct value from the normalized DQ buildup.

Even more striking results are obtained for the "slow" correlation times, which are plotted in Figure 7b. The results for the different data sets differ by 1−2 orders of magnitude, explaining why *simultaneous* fits did not satisfactorily agree with the data at any temperature. The τ_s obtained from $I_{\Sigma MQ}$ are in the range of microseconds. If the residual dipolar tensor underwent isotropic rotational diffusing with such a time constant, a DQ buildup could not possibly be observed on the time scale of some milliseconds! Most perturbingly, the apparent correlation times increase with increasing temperature, which is completely unphysical. Therefore, the slow-motion model, which was used in a large number of publications, is to be dismissed for the analysis of transverse relaxation phenomena in elastomers.

Fast-Motion Model. These major problems are fixed when we take the fast segmental motions as the dominant source of relaxation. The simplest *ansatz* is to assume rotational diffusion of the intrasegmental static-limit tensor (characterized by M_{2eff}), where a weak residual degree of anisotropy is introduced via S_b. This situation is modeled by the ACF eq 19. Starting with eqs 11 and 12 and going through the mathematics related to integrals over correlation functions is a straightforward exercise, and the results are

$$I_{DQ} = \exp\left\{-\frac{8}{9}(1-S_b^2)M_{2eff}\tau_f^2\left(e^{-\tau_{DQ}/\tau_f}+\frac{\tau_{DQ}}{\tau_f}-1\right)-\frac{4}{9}S_b^2M_{2eff}\tau_{DQ}^2\right\}\sinh\left\{\frac{4}{9}(1-S_b^2)M_{2eff}\tau_f^2(e^{-2\tau_{DQ}/\tau_f}-2e^{-\tau_{DQ}/\tau_f}+1)+\frac{4}{9}S_b^2M_{2eff}\tau_{DQ}^2\right\} \quad (28)$$

$$I_{\Sigma MQ} = \exp\left\{-\frac{4}{9}(1-S_b^2)M_{2eff}\tau_f^2\left(4e^{-\tau_{DQ}/\tau_f}-e^{-2\tau_{DQ}/\tau_f}+\frac{2\tau_{DQ}}{\tau_f}-3\right)\right\} \quad (29)$$

Note that eq 29 is formally, apart from the prefactor of M_{eff}, equivalent to eq 26, which reflects the fact that the static contribution is in either case fully refocused. In other words, fits to $I_{\Sigma MQ}$ or other dipolar-refocused relaxation decays (such as mixed magic echoes[23]) alone cannot be used to verify or falsify the form of the ACF.

Combined Model. As a further step, the residual tensor can be assumed to be subject to additional slow exponential loss of correlation by cooperative motions. Equation 20 describes this scenario. It is essentially the same ACF that is the core of the famous Lipari−Szabo model for the description of relaxation of (biological) macromolecules in solution subject to fast internal fluctuations and slower overall tumbling.[33] Many of its properties and limits of applicability (most importantly the condition $\tau_s \gg \tau_f$) are comprehensively discussed in their encyclopedic publication. Notably, they found that S_b is always a stable result even in cases where the specific form of the ACF is not known a priori. S_b can of course in our case be determined independently (from I_{nDQ}), while it is a fitting parameter in solution

CDV

experiments, where the global mobility described by τ_s is still much faster than the time scale set by the couplings. For this model, the signal functions are again obtained in an analogous manner and are basically combinations of the above two cases:

$$I_{DQ} = \exp\left\{-\frac{8}{9}(1-S_b^2)M_{2eff}\tau_f^2\left(e^{-\tau_{DQ}/\tau_f}+\frac{\tau_{DQ}}{\tau_f}-1\right)-\frac{8}{9}S_b^2M_{2eff}\tau_s^2\left(e^{-\tau_{DQ}/\tau_s}+\frac{\tau_{DQ}}{\tau_s}-1\right)\right\}\sinh\left\{\frac{4}{9}(1-S_b^2)M_{2eff}\tau_f^2(e^{-2\tau_{DQ}/\tau_f}-2e^{-\tau_{DQ}/\tau_f}+1)+\frac{4}{9}S_b^2M_{2eff}\tau_s^2(e^{-2\tau_{DQ}/\tau_s}-2e^{-\tau_{DQ}/\tau_s}+1)\right\} \quad (30)$$

$$I_{\Sigma MQ} = \exp\left\{-\frac{4}{9}(1-S_b^2)M_{2eff}\,\tau_f^2\left(4e^{-\tau_{DQ}/\tau_f}-e^{-2\tau_{DQ}/\tau_f}+\frac{2\tau_{DQ}}{\tau_f}-3\right)-\frac{4}{9}S_b^2M_{2eff}\tau_s^2\left(4e^{-\tau_{DQ}/\tau_s}-e^{-2\tau_{DQ}/\tau_s}+\frac{2\tau_{DQ}}{\tau_s}-3\right)\right\} \quad (31)$$

Power-Law Model. Finally, we test

$$C(t) = \begin{cases} 1 & \text{for } |t| < \tau_0 \\ (1-S_b^2)(\tau_0/|t|)^\kappa + S_b^2 & \text{for } |t| \geq \tau_0 \end{cases} \quad (32)$$

as a model for the fast initial decay. Kimmich and co-workers have proposed such an approach for a more realistic account of polymer dynamics, where superpositions of processes on different time scales (e.g., Rouse modes) must commonly be expected.[34] In their work on the dipolar correlation effect in rubbers,[12] they have however used such a function to model the alleged *slow* process, and our corresponding tests showed that this leads to the same unphysical temperature dependence that we have observed for the exponential slow-motion ACF. Using eq 32 for the *fast* decay, we obtain

$$I_{DQ} = \exp\left\{-\frac{\frac{4}{9}(1-S_b^2)M_{2eff}}{(\kappa-2)(\kappa-1)}\left(\kappa\left(2(\kappa-2)\frac{\tau_{DQ}}{\tau_0}-(\kappa-1)\right)\tau_0^2+2\tau_{DQ}^{2-\kappa}\tau_0^\kappa\right)-\frac{4}{9}S_b^2M_{2eff}\tau_{DQ}^2\right\}\sinh\left\{\frac{\frac{4}{9}(1-S_b^2)M_{2eff}}{2(\kappa-2)(\kappa-1)}(\kappa(\kappa-1)\tau_0^2-2^{2-\kappa}(2^\kappa-2)\tau_{DQ}^{2-\kappa}\tau_0^\kappa)+\frac{4}{9}S_b^2M_{2eff}\tau_{DQ}^2\right\} \quad (33)$$

$$I_{\Sigma MQ} = \exp\left\{-\frac{\frac{4}{9}(1-S_b^2)M_{2eff}}{(\kappa-2)(\kappa-1)}\left(\tau_0^2\kappa\left(2(\kappa-2)\frac{\tau_{DQ}}{\tau_0}-\frac{3}{2}(\kappa-1)\right)+4\tau_{DQ}^{2-\kappa}\tau_0^\kappa(1-2^{-\kappa})\right)\right\} \quad (34)$$

These relations are valid under the conditions $\kappa > 0$, $\kappa \neq 1, 2$, and $\tau_0 < \tau_{DQ}$. The latter is not very restrictive under realistic experimental conditions, where the minimum accessible τ_{DQ} is on the order of tens of microseconds, while the onset time τ_0 is orders of magnitude shorter.

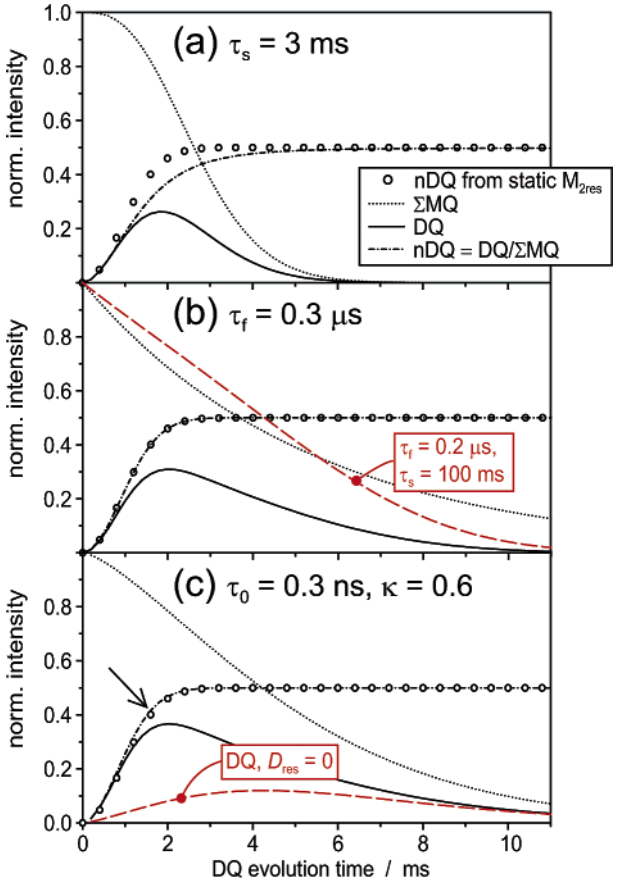

Figure 8. Intensity data for MQ experiments calculated on the basis of the different ACFs: (a) slow-motion model, eqs 25 and 26; (b) fast-motion model, eqs 28 and 29, and $I_{\Sigma MQ}$ for the composite model, eq 31; and (c) power-law model, eqs 33 and 34. In all cases, the DQ buildup data are compared with the buildup based on a quasi-static second moment, eq 3, and the analytical normalized $I_{nDQ} = I_{DQ}/I_{\Sigma MQ}$. Other parameters are $D_{stat}/k = 2\pi \times 6300$ rad/s and $D_{res} = 2\pi \times 200$ rad/s ($S_b = 0.032$). The dashed lines in (b) and (c) correspond to results using different (boxed) parameters and are described in the text.

Comparison of Model Predictions. The qualitative features of MQ data calculated on the basis of the different models can be inspected in Figure 8. The couplings are chosen on the basis of the experimental findings, and the correlation times are selected so as to qualitatively reproduce the experimental trends for both I_{DQ} and $I_{\Sigma MQ}$ of NR-A3 at a temperature of about 320 K, where I_{DQ} reaches a maximum of about 0.3 at $\tau_{DQ} = 2$ ms.

In Figure 8a, it is shown that Gaussian-type decays of $I_{\Sigma MQ}$ would be expected for the unrealistic slow-motion model. In addition, the normalization procedure should fail, as the analytical I_{nDQ} falls below the quasi-static prediction and thus depends on τ_s. This is again in contrast to the experimental finding that I_{nDQ} is nearly independent of temperature.

From Figure 8b, we take the confirmation that a dominant fast process does not exert an influence on I_{nDQ}; normalization is successful. In this range, eqs 25 and 26 predict a nearly exponential transverse relaxation behavior, which is equal for the two signal functions and thus cancels upon division. For $\tau_{DQ}/\tau_f \gg 1$, we find that $I_{\Sigma MQ}$ is reduced to

$$I_{\Sigma MQ} = \exp\left\{-\frac{8}{9}(1-S_b^2)M_{2eff}\tau_f\tau_{DQ}\right\} \quad (35)$$

CDV

while I_{DQ} is equal to eq 3 multiplied by this exponential loss term. The apparent fast-limit MQ relaxation time is thus

$$T_{2MQ} = \left(\frac{8}{9}(1 - S_b^2)M_{2eff}\tau_f\right)^{-1} \approx 2.5\left(\frac{D_{stat}}{k}\right)^{-2}\tau_f^{-1} \quad (36)$$

Note that, apart from the square dependence of S_b, this result is identical to the exponential loss term derived for the dipolar dephasing function, eq 24. For $S_b \rightarrow 0$, both results match, as expected, and the difference is rather minor for experimentally relevant S_b in the percent range. A relaxation term of similar form was predicted by Brereton for the case of transverse relaxation of Rouse chains in melts and networks.[24,29] In this case, $(1 - S_b^2)M_{2eff}$ was associated with the coupling within the so-called "NMR submolecule",[3] similar to using a pre-averaged $M_{2eff} \sim (D_{stat}/k)^2$ for the Kuhn segment, and τ_f was associated with the fastest Rouse mode.

Experimentally, however, only the lowest temperature results (see Figure 2) exhibit exponential relaxation behavior. At higher temperatures, the shape of $I_{\Sigma MQ}$ becomes increasingly convex, and several causes appear possible:

(i) Isotropic J couplings, which are always part of the total average Hamiltonian, can become observable because $[\bar{H}_D,\hat{H}_J] \neq 0$.[35] In weakly coupled multispin systems where D is only about 10 times larger than J, dipolar J cross-terms indeed lead to a notable parabolic dephasing of a dipolar-refocused intensity. Fortunately, exemplary spin dynamics simulations of an NR monomer unit[4] with typical dipolar and J couplings indicate that this loss is on the 10% scale within $\tau_{DQ} \leq 5$ ms and is thus hardly relevant here. The effect may, however, become important in more weakly coupled entangled polymers. Note that this must also be taken into account for rubbers with chemically equivalent protons such as PDMS. This somewhat counterintuitive behavior can superficially be explained by the fact that a dipolar coupling renders two otherwise equivalent spins magnetically *inequivalent* in the same way as a relative chemical shift (the formal derivation involves the above commutator).

(ii) Additional loss of correlation below S_b^2 might play a role. This is indicated by the dashed line in Figure 8b, where a τ_s of 100 ms was additionally considered.

(iii) More convex relaxation curves are also obtained when considering the power-law ACF (see Figure 8c). In this case, we highlight the very interesting finding that I_{DQ} does not vanish even for $D_{res} = S_b = 0$. This explains why I_{nDQ} even slightly surpasses the static-limit buildup curve (indicated by the arrow). This is because correlations decaying by power laws persist over much longer time scales than in the exponential case. For example, for the parameters given in Figure 8b,c, the exponential ACF decays to about 0.001 after 2 ms, while the power-law ACF is still 5 times higher and decays further by less than factor of 2 within the next 2 ms.

Therefore, when one accepts that power laws could correctly model the correlation loss of segments subject to polymer dynamics over large time scales, it is possible that even the normalized DQ buildup is in part influenced by processes which involve length scales that are significantly smaller than the cross-link separations. Our comparison of network and linear chain data to be presented below corroborates this finding.

Application to Experimental Data. In Figure 9, we show the analysis of experimental DQ and ΣMQ intensities using the improved models. The fits were in each case performed *simultaneously* to both sets of data. As M_{2eff} is fixed, there are only two or three free parameters each, which provides stable fitting in most cases even when the functional form of the fitting functions cannot fully reproduce the data. The results for all

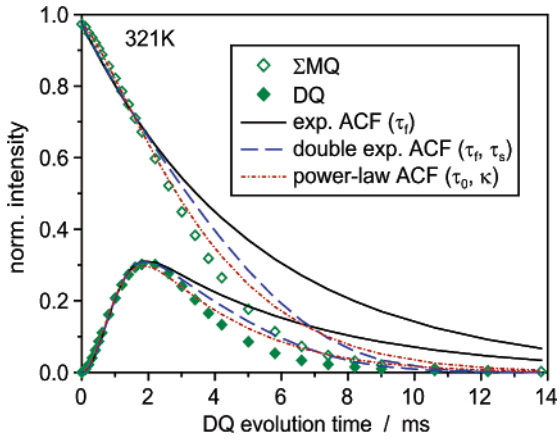

Figure 9. MQ data acquired for NR-A3 at 321 K and fitting results. For the three improved models, eqs 28 and 29, eqs 30 and 31, and eqs 33 and 34, respectively, where fitted simultaneously to the two sets of data.

investigated temperatures are listed in Table 1. The fitting accuracy for the exponent κ was generally not very high (about ± 0.05), and at higher temperatures, i.e., where the ΣMQ relaxation curves become increasingly convex, we observed increasing interdependencies between τ_0 and κ. The variations in τ_0 over a range of similarly low χ^2 were however not larger than the last significant digit given. Note that, following eq 15, fitting was only performed up to $\tau_{DQ} = 1.8$ ms. The long-time behavior can be considered a prediction, and one should bear in mind that the more efficient correlation loss of increasingly important higher-spin coherences requires that experimental data should always lie below these lines, as is observed.

In accordance with the above discussion, the model considering only τ_f fails to reproduce the convexity of the ΣMQ relaxation, and the addition of both a slow exponential process and the power-law model does better in capturing this feature. Reassuringly, however, both the single- and double-exponential model yield very similar results for τ_f (see Table 1). Yet, τ_s still exhibits an unphysical increase with temperature, again indicating that isotropic rotational diffusion is inappropriate to describe an assumed cooperative long-time behavior. The power-law model clearly works best, and it does not require any assumptions on such a long-time process. In fact, the ^{2}H spin-alignment experiments of Sotta and Deloche on PDMS networks at room temperature suggest that such a process should be absent up to about 300 ms.[36]

Finally, Figure 10 shows the new results for τ_f and τ_0 in comparison to the unphysical τ_s discussed in the context of Figure 7b. Both quantities vary over orders of magnitude in the investigated temperature range and exhibit a characteristic upturn upon approaching T_g, suggesting that the association of the dominant relaxation process with fast and more local segmental motions is correct. The τ_f can even be fitted to a WLF function, and the extrapolated glass transition matches the DSC value within 1 K. The unrealistically small value of $\tau_f(T_g) = 35.2$ ms however, shows that rotational diffusion is certainly a rather crude model to describe the multi-time-scale nature of polymer motion.

While the power law might model the real behavior better, we still lack the theoretical understanding to attach physical significance to the onset time τ_0 and the exponent κ. In particular, the T dependence of τ_0 cannot be satisfactorily described by the WLF function. The work of Kimmich suggests that the true ACF might in fact follow different power laws over different time regimes,[34] and we hope that future theoretical

CDV

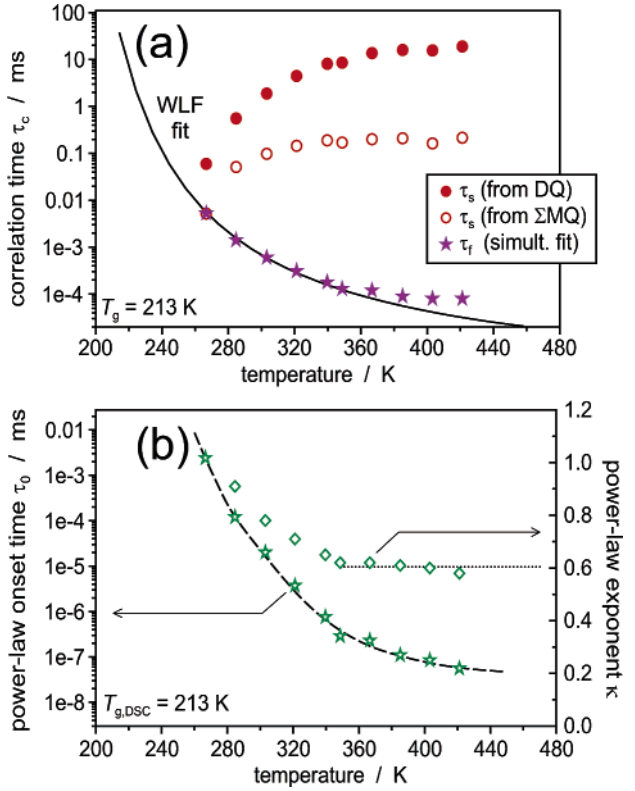

Figure 10. Comparative plots of the correlation times obtained from the different fits to data for NR-A3. In (a), τ_f is compared to the different τ_s of Figure 7b. The line is a WLF fit using the canonical values for the constants,[37] and $\tau_f(T_g) = 35.2$ ms and $T_g = 214$ K as results. Part (b) shows the onset times τ_0 and the exponent κ for the power-law ACF.

work will reveal the true shape of network chain ACFs and thus help to obtain a more quantitative picture.

D. Comparison of Network and Melt Dynamics. Figure 11 highlights the qualitative differences between MQ data from networks and linear-chain melts. The MQ technique has early on been shown to provide insight into large-scale chain motion (i.e., reptation) and entanglement-induced local chain ordering in poly(butadiene) melts by Graf, Heuer, and Spiess,[5] and we are now in a position to refine some of the previous arguments.

Note first that linear natural rubber is a complex material that is not completely soluble (probably due to some oxygen-induced cross-linking) and appears to exhibit physical cross-links of an origin unknown to us. We found that the NMR behavior was history-dependent, in that for instance a sample of NR-lin heated to 350 K showed a higher chain order than one that was heated to 430 K for about 10 min prior to the same experiment. The presented data are based on the latter type of thermal treatment. (In the networks, such differences were not observed, but longer heating at higher temperatures did lead to irreversible changes.) We here just take NR-lin as representative of a linear polymer that offers the (partial) possibility for large-scale chain motion. More quantitative studies will have to be performed on properly calibrated samples.

The most important observation in Figure 11a is the initial-rise behavior of both I_{DQ} and I_{nDQ}: while it is nearly T-independent in the network, it is slower and varies strongly for the melt, thus identifying an important NMR signature of reptational dynamics. To the contrary, the overall correlation loss as reflected in the relaxation behavior of $I_{\Sigma MQ}$ is similar in the two cases, suggesting that transverse relaxation in the entangled melt is still significantly influenced by fast segmental

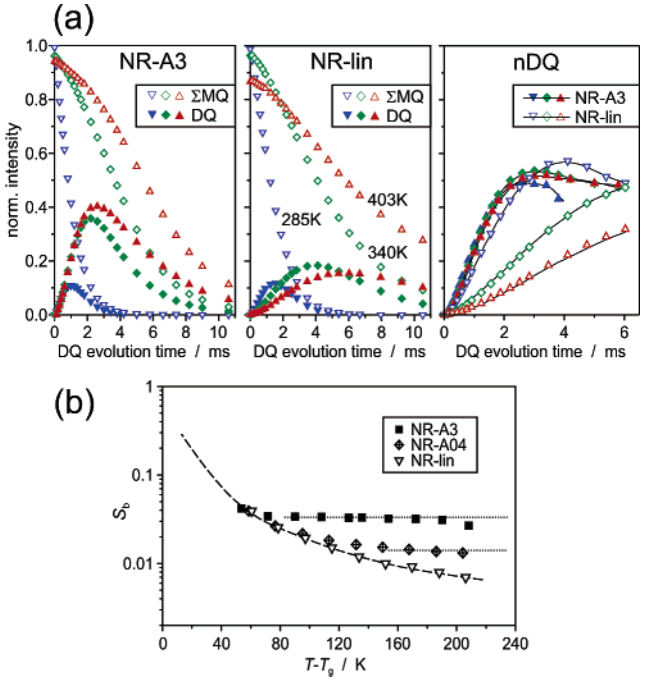

Figure 11. (a) Comparison of the MQ signal functions of NR-A3, a highly cross-linked network, and NR-lin, the linear precursor melt, at different temperatures. (b) Results for S_b from fits to I_{nDQ} using eq 3 for $I_{nDQ} \leq 0.45$. For NR-lin at temperatures >360 K, the fitting limit was $I_{nDQ} \leq 0.25$.

motions. This may complicate the reliable separation of segmental and reptation-type contributions in transverse relaxation experiments.[26]

As seen above, the influence of these fast processes is at least partially removed by normalization, suggesting that the remaining T-dependent decrease of I_{nDQ} is indicative of larger-scale motion only. This justifies in retrospect the results of Graf et al., who have assumed that for short times

$$I_{nDQ} \approx \frac{1}{5} D_{res}^{\ 2} \tau_{DQ}^{\ 2} C(t/t_e) \qquad (37)$$

where $C(t/t_e)$ should subsume correlation loss due to slow processes on a length scale of the reptation tube diameter a and above (i.e., processes that are slower than the equilibration time τ_e). Using a fixed reference value for D_{res} that was determined at $T \approx T_g + 50$ K (below which the signal was observed to be independent of molecular weight), they could indeed qualitatively confirm the power-law behavior that is predicted for $C(t/t_e)$ in the framework of the tube model.[38]

A yet unexplained and much debated finding was the surprisingly high value of D_{res} determined in this and also other previous papers.[5,39,40] It corresponded to an S_b of about 0.2, while it was expected to attain a value typical for dynamic averaging on the length scale of a, i.e., for interentanglement spacings, where $S_b \approx 0.01$. This discrepancy is at least to a large part explained by the S_b which are plotted in Figure 11b. While for NR-A3, a plateau is reached at about 60 K above T_g, S_b continues to decrease for NR-A04 and NR-lin over a much wider range.

The sample NR-A04 is rather lowly cross-linked, and from our previous work, we infer that chain order in this sample is not significantly larger than the entanglement-induced order (the cross-link separations M_c are larger than M_e), while reptation should be suppressed.[4] Yet still, S_b continues to decrease at temperatures as high as 160 K above T_g, indicating that the effect

of fast segmental averaging on I_{nDQ} is not complete even at these temperatures!

We now come back to the above discussion of the properties of the theoretical MQ signal behavior for the case of a power-law correlation function (Figure 8c), where even without an apparent S_b residual chain order is detectable. As mentioned above, this is due to the slowly decaying nature of the ACF; its long tail appears to be more and more important when the piece of chain that is unperturbed by cross-links becomes larger and has to explore an increasingly large conformational space. The corresponding additional contribution to I_{nDQ} and thus to S_b would naturally decrease when the local processes are sped up at higher T. We hypothesize that the very weak trend of S_b as determined from I_{nDQ} for NR-A3 toward lower values at higher temperature is also due to this effect.

Support of this scenario can be taken from a recent collaboration with J.-U. Sommer, who investigated residual order in Monte Carlo simulations of end-linked networks and found that the tensorial self-averaging as expressed by the dipolar phase factor, eq 8, which expresses a running time average, exhibits a power-law behavior that is indeed much retarded as compared to a vectorial bond order parameter.[32] It still remains to be investigated in how far this extends also to the ACF of P_2, eq 16.

In conclusion, we explain the unusually high chain order observed by Spiess and co-workers by incomplete segmental averaging between entanglement constraints and the corresponding additional contribution to the residual dipolar coupling detected via I_{nDQ}. Accepting this explanation, it is clear that the NMR observable S_b cannot be expected to simply represent chain order between fixed constraints. In other words, the assumption that neglects segmental dynamics on a length scale shorter than a cannot be expected to hold a priori, neither for the overall transverse relaxation behavior in networks nor for the coherently detected order parameter in networks or melts. The only reliable strategy to attach length-scale information to the observed chain order is therefore the observation of temperature independence in moderately to highly cross-linked networks and to extrapolate to zero cross-links to obtain the entanglement contribution.[4] For melts, this is an open challenge, as the self-averaging behavior induced by reptation and its interference with the long tail of the segmental relaxation is not yet understood.

Future work will have to show to which extent the phenomenology of Figure 11b is also observed for other polymer systems and in how far correlations to well-known parameters of the tube models (e.g., the friction coefficient, the entanglement molecular weight) and the processes governing the glass transition can be established. Improved models for the analysis of MQ and other NMR experiments of polymers above T_g will have to incorporate the full spectrum of motions starting at the segmental level and take into account the peculiarities of the tensorial self-averaging process that are central to the average Hamiltonian and AW treatments.

The work of Brereton on analytical solutions for Hahn-echo decays appears promising in this regard,[24] as it is the only *ansatz* that explicitly considers fast segmental motions as an important source of relaxation and also provides an alternative to AW. We however note again that, experimentally, we could not support the very central assumption of this and earlier theories that the Gaussian end-to-end distance distribution of chains between topological constraints has a direct influence on the data, i.e., should lead to a gamma distribution of residual couplings and to accordingly stretched nDQ buildup curves.[4,8,32] Therefore, the significance of Cohen-Addad's "NMR submolecule" that is usually evoked to establish statistical scale invariance,[3] in particular its relation to the Kuhn segment size and the tube diameter a, will have to be considered carefully in light of these findings.

4. Conclusions

In summary, we have shown that the slow-motion scenario that was used in many models for the analysis of NMR data of polymer networks and melts does not hold in general. We have discussed the advantages of static MQ spectroscopy in the context of the NMR analysis of networks, where it became clear that the analysis of two independent sets of data, i.e., I_{DQ} and $I_{\Sigma MQ}$, and their comparison to Hahn-echo decay functions, can be used to investigate the range of applicability of the Andersen−Weiss approximation that permits the derivation of closed-form signal functions on the basis of specific models for the segmental orientation autocorrelation function. The applicability of the individual models can be tested by simultaneous fits to the two signal functions, and in this way, we could show that the slow-motion *ansatz* that models the loss of spin−spin correlation solely on the basis of large-scale cooperative rearrangements on the length scale of cross-links is not applicable.

The time scale of fast segmental motions providing the preaveraging of tensorial NMR interactions clearly dominates the relaxation process, yet the explicit functional form of the correlation function describing these motions is not known at present. While an exponential loss of correlation yields correlation times that correlate well with the WLF function describing the slowdown upon approaching T_g, the correlation of the obtained values for the fast correlation time with the parameters from established theories of polymer dynamics is unclear. The experimental intensity decay appears parabolic at higher temperatures, and power laws describe this feature best and do not rely on assumptions on slow large-scale rearrangements, the existence and importance of which for NMR observables are not confirmed. It should, however, be kept in mind that experimental tests of improved models might be challenged by the possible influence of J couplings, which lead to a weak additional parabolic signal dephasing and must be carefully considered.

Finally, a comparison of the NMR response of networks and a linear-chain melt showed that the large-scale motions characteristic for a melt, as for instance described by the tube and reptation models, imparts a clear signature on the time and temperature dependence of the dynamic chain order parameter, yet they do not appreciably change the overall relaxation behavior, which is still dominated by the segmental process. In further contradiction to the slow-motion model, the magnitude of the NMR-detected order parameter is also influenced by local segmental processes that occur below the entanglement length scale, thus explaining the unusually high order parameters reported in some earlier publications. Future work will be directed at the development of more appropriate models for the NMR analysis of polymer networks and melts, where a detailed and quantitative correlation of NMR observables with established polymer models, on one hand, and observables from experiments such as dielectric relaxation, rheology, or neutron scattering, on the other hand, is still an open challenge.

Acknowledgment. Funding of this work was provided by the Deutsche Forschungsgemeinschaft (SFB 428) and the Fonds der Chemischen Industrie. We thank Robert Graf, Paul Cal-

CDV

laghan, and Rainer Kimmich for stimulating discussions and fruitful comments. Jörn Schmedt auf der Günne is thanked for pointing out the significance of *J* couplings and M. A. López-Manchado and B. Herrero for providing the samples.

Appendix. Cycle Time Dependence

We here give a short review of our previously published treatment of correlation loss during finite evolution delays which make up an actual MQ pulse sequence[10] and summarize the differences that arise in the context of different correlation functions. The essential starting point is that the repetitive pulse sequence cycle of length t_c (that is repeated n_c times to realize a specific τ_{DQ}) is subdivided into specific evolution periods between pulses. The pulses are treated as infinitely short, which should not be a large restriction except for experimentally irrelevant duty cycles, as discussed previously. When one considers explicitly the terms that make up the average Hamiltonian, the integral in the calculation of the double-quantum phase (eq 8) is to be performed in discrete steps which cover only those intervals (t_i, t_j) during which the magnetization is formally transverse:

$$\phi_{DQ} = \frac{3}{2} D_{eff} \sum_{intervals} \int_{t_i}^{t_j} P_2(\cos \beta_t)\, dt \qquad (A.1)$$

This then necessitates a careful treatment of the averages over products of such phase factors which are performed to obtain the signal functions according to eqs 11 and 12. The resulting double integrals over the correlation function, as for example given by eq 17, thus turn into more involved combinations of double sums and integrals, where the resulting integrals heuristically correspond to evaluating the correlation loss within and between individual transverse evolution periods.

We refrain from reporting the algebraically complex signal functions for all considered model ACFs and restrict ourselves to the presently most useful case for the analysis of experimental data. The final t_c-dependent results for I_{DQ} and $I_{\Sigma MQ}$, eqs 11 and 12, for the exponential correlation function that models the fast initial decay, eq 19, read

$$I_{DQ}^{(t_c)} = \frac{1}{2}\exp\{-(1-S_b^{\,2})M_{2eff}\tau_c^{\,2}(A+B)\} - \frac{1}{2}\exp\{-(1-S_b^{\,2}) M_{2eff}\tau_c^{\,2}(A+C)\}\exp\left\{-\frac{8}{9}S_b^{\,2}M_{2eff}t_c^{\,2}n_c^{\,2}\right\} \qquad (A.2)$$

and

$$I_{\Sigma MQ}^{(t_c)} = \exp\{-(1-S_b^{\,2})M_{2eff}\tau_c^{\,2}(A+B)\} \qquad (A.3)$$

where

$$A = 8n_c\left(e^{-t_c/6\tau_c} + \frac{t_c}{6\tau_c} - 1\right) \qquad (A.4)$$

$$B = \left(2\cosh\left(\frac{t_c}{6\tau_c}\right) - 2\right)\sum_{i=1}^{4n_c}[(8n_c - 3i)e^{-it_c/4\tau_c} - (4n_c - i)e^{-(i+4n_c)t_c/4\tau_c}] \qquad (A.5)$$

$$C = \left(2\cosh\left(\frac{t_c}{6\tau_c}\right) - 2\right)\sum_{i=1}^{4n_c}[(8n_c - i)e^{-it_c/4\tau_c} + (4n_c - i)e^{-(i+4n_c)t_c/4\tau_c}] \qquad (A.6)$$

These relations reduce to eqs 28 and 29 in the continuous limit ($n_c \to \infty$, $t_c \to 0$, $\tau_{DQ} = n_c t_c = \text{const}$). Term *A* corrects an error in eq 32 of ref 10, where the factor 16 has to be replaced by 8. This previous equation was derived on the basis of the slow-motion model and that the second moment was defined in a different way. Thus, $(1 - S_b^{\,2})M_{2eff}$ is to be replaced by $^9/_4\delta M_2^{DQ}$ for a proper comparison with eq A.3. Note that for a numerically stable implementation of the sums in eqs A.5 and A.6, the cosh function needs to be expanded in terms of its constituent exponentials and multiplied into the sums, such that the argument $(t_c/6\tau_c)$ is combined with the *i*-dependent arguments before exponentiation.

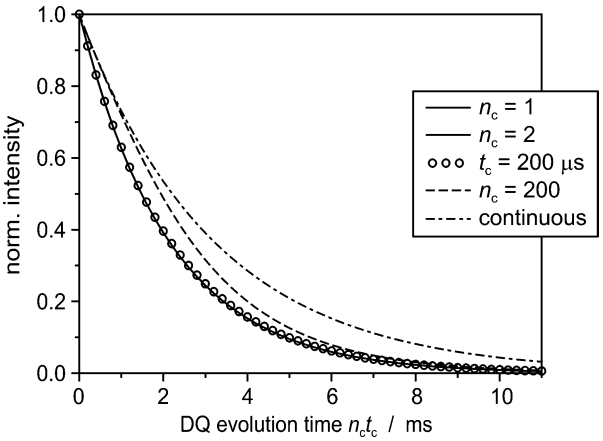

Figure 12. Changes in the relaxation behavior of $I_{\Sigma MQ}$ in MQ experiments with finite numbers of pulse sequence cycles according to eq A.3. The parameters are $D_{stat}/k = 2\pi \times 6300$ rad/s, $S_b = 0.032$, and $\tau_f = 0.5$ μs.

The error then suggested apparently stronger finite-cycle effects than actually expected from the now corrected treatment. In the (now obsolete) slow-motion region discussed in Figure 4 of ref 10, the corrected time scale of signal decay only decreases by about 10% upon transition from a continuous treatment ($t_c \to 0$) to a time-incremented experiment with $n_c = 1$. Larger differences are found in the fast-motion domain, which is more relevant for the data discussed in this paper.

Figure 12 demonstrates the differences between the continuous case and a single time-incremented cycle. Except for the (experimentally hardly relevant) case of $n_c = 200$, all curves are almost perfectly exponential, and the apparent transverse relaxation time (T_{2MQ}) differs by a factor of 1.5 between the limits. The lowest experimentally feasible cycle time is on the order of 200 μs, and the relaxation behavior is then seen to be rather close to experiments with one or two time-incremented cycles, as performed on the minispec. As discussed in the context of eq 36, $\tau_f \propto T_{2MQ}^{-1}$. Thus, a factor of 1.5 should be used to correct any of the fitted quantities for finite-t_c effects.

Experimentally, we found that fits using eqs A.2 and A.3 yielded values for τ_f which were about 1.4 times smaller than the values reported in Table 1, in agreement with the theoretical expectation. Finally, a similar comparative analysis of the experimental data involving finite-t_c expressions on the basis of the power-law ACF gave roughly the same exponents κ and onset times τ_0 which were also between 1.4 and 1.5 times smaller than those reported for the continuous treatment.

References and Notes

(1) Litvinov, V. M., De, P. P., Eds.; *Spectroscopy of Rubbers and Rubbery Materials*; Rapra Technology Ltd.: Shawbury, 2002.
(2) Cohen-Addad, J. P. Method of measurement of nonzero average dipolar spin coupling in molten polymers. *J. Chem. Phys.* **1975**, *63*, 4880−4885.

(3) Cohen-Addad, J. P. NMR and Fractal Properties of Polymeric Liquids and Gels. *Prog. NMR Spectrosc.* **1993**, *25*, 1−316.
(4) Saalwächter, K.; Herrero, B.; López-Manchado, M. A. Chain order and crosslink density of elastomers as investigated by proton multiple-quantum NMR. *Macromolecules* **2005**, *38*, 9650−9660.
(5) Graf, R.; Heuer, A.; Spiess, H. W. Chain-Order Effects in Polymer Melts Probed by ^{1}H Double-Quantum NMR Spectrocopy. *Phys. Rev. Lett.* **1998**, *80*, 5738−5741.
(6) Graf, R.; Demco, D. E.; Hafner, S.; Spiess, H. W. Selective residual dipolar couplings in cross-linked elastomers by ^{1}H double-quantum NMR spectroscopy. *Solid State Nucl. Magn. Reson.* **1998**, *12*, 139−152.
(7) Schneider, M.; Gasper, L.; Demco, D. E.; Blümich, B. Residual dipolar couplings by ^{1}H dipolar-encoded longitudinal magnetization, double- and triple-quantum nuclear magnetic resonance in cross-linked elastomers. *J. Chem. Phys.* **1999**, *111*, 402−415.
(8) Saalwächter, K.; Ziegler, P.; Spyckerelle, O.; Haidar, B.; Vidal, A.; Sommer, J.-U. ^{1}H multiple-quantum nuclear magnetic resonance investigations of molecular order distributions in poly(dimethylsiloxane) networks: Evidence for a linear mixing law in bimodal systems. *J. Chem. Phys.* **2003**, *119*, 3468−3482.
(9) Saalwächter, K. Detection of Heterogeneities in Dry and Swollen Polymer Networks by Proton Low-Field NMR Spectroscopy. *J. Am. Chem. Soc.* **2003**, *125*, 14684−14685.
(10) Saalwächter, K. ^{1}H multiple-quantum nuclear magnetic resonance investigations of molecular order in polymer networks: II. Intensity decay and restricted slow dynamics. *J. Chem. Phys.* **2004**, *120*, 454−664.
(11) Kimmich, R. *NMR Tomography, Diffusometry, Relaxometry*; Springer: Berlin, 1997.
(12) Fischer, E.; Grinberg, F.; Kimmich, R.; Hafner, S. Characterization of polymer networks using the dipolar correlation effect on the stimulated echo and field-cycling nuclear-magnetic resonance relaxometry. *J. Chem. Phys.* **1998**, *109*, 846−854.
(13) Kariyo, S.; Stapf, S. Influence of Cross-Link Density and Deformation on the NMR Relaxation Dispersion of Natural Rubber. *Macromolecules* **2002**, *35*, 9253−9255.
(14) Kariyo, S. Stapf, S.; Blümich, B. Site specific proton and deuteron NMR relaxation dispersion in selectively deuterated polyisoprene melts. *Macromol. Chem. Phys.* **2005**, *206*, 1292−1299.
(15) Gotlib, Yu. Ya.; Lifshitz, M. I.; Shevelev, V. A.; Lishanskij, I. S.; Balanina, I. V. *Vysokomol. Soedin.* **1976**, *10*, 2299.
(16) Sotta, P.; Fülber, C.; Demco, D. E.; Blümich, B.; Spiess, H. W. Effect of Residual Dipolar Interactions on the NMR Relaxation in Cross-Linked Elastomers. *Macromolecules* **1996**, *29*, 6222−6230.
(17) Knörgen, M.; Menge, H.; Hempel, G.; Schneider, H.; Ries, M. E. Relationship between the transverse NMR decay and the dipolar interaction in elastomers: a comparison of two models. *Polymer* **2002**, *43*, 4091−4096.
(18) Saalwächter, K.; Klüppel, M.; Luo, H.; Schneider, H. Chain Order in Filled SBR Elastomers: A Proton Multiple-Quantum NMR Study. *Appl. Magn. Reson.* **2004**, *27*, 4071−417.
(19) Saalwächter, K. Artifacts in Transverse Proton NMR Relaxation Studies of Elastomers. *Macromolecules* **2005**, *38*, 1508−1512.
(20) Collignon, J.; Sillescu, H.; Spiess, H. W. Pseudo-solid echoes of proton and deuteron NMR in polyethylene melts. *Colloid Polym. Sci.* **1981**, *259*, 220−226.
(21) Callaghan, P. T.; Samulski, E. T. Molecular Ordering and the Direct Measurement of Weak Proton−Proton Dipolar Interactions in a Rubber Network. *Macromolecules* **1997**, *30*, 113−122.
(22) Grinberg, F.; Garbarczyk, M.; Kuhn, W. Influence of the cross-link density and the filler content on segment dynamics in dry and swollen natural rubber studied by the NMR dipolar-correlation effect. *J. Chem. Phys.* **1999**, *111*, 11222−11231.
(23) Fechete, R.; Demco, D. E.; Blümich, B. Chain orientation and slow dynamics in elastomers by mixed magic-Hahn echo decays. *J. Chem. Phys.* **2003**, *118*, 2411−2421.
(24) Brereton, M. G. NMR Transverse Relaxation Function Calculated for Constrained Polymer Chains: Application to Entanglements and Networks. *Macromolecules* **1990**, *23*, 1119−1131.
(25) Brereton, M. G.; Ward, I. M.; Boden, N.; Wright, P. Nature of Proton NMR Transverse Relaxation Function of Polyethylene Melts. 1. Monodispersed Polyethylenes. *Macromolecules* **1991**, *24*, 2068−2074.
(26) Klein, P. G.; Adams, C. H.; Brereton, M. G.; Ries, M. E.; Nicholson, T. M.; Hutchings, L. R.; Richards, R. W. Rouse and Reptation Dynamics of Linear Polybutadiene Chains Studies by ^{2}H NMR Transverse Relaxation. *Macromolecules* **1998**, *31*, 8871−8877.
(27) Ball, R. C.; Callaghan, P. T.; Samulski, E. T. A simplified approach to the interpretation of nuclear spin correlations in entangled polymeric liquids. *J. Chem. Phys.* **1997**, *106*, 7352−7361.
(28) Andersen, P. W.; Weiss, P. R. Exchange Narrowing in Paramagnetic Resonance. *Rev. Mod. Phys.* **1953**, *25*, 269−276.
(29) Brereton, M. G. NMR Transverse Relaxation Function Calculated for the Rouse Model. *Macromolecules* **1989**, *22*, 3667−3674.
(30) Baum, J.; Pines, A. Multiple-Quantum NMR Studies of Clustering in Solids. *J. Am. Chem. Soc.* **1986**, *108*, 7447−7454.
(31) Saalwächter, K.; Kleinschmidt, F.; Sommer, J.-U. Swelling Heterogeneities in End-Linked Model Networks: A Combined Proton Multiple-Quantum NMR and Computer Simulation Study. *Macromolecules* **2004**, *37*, 8556−8568.
(32) Sommer, J.-U.; Saalwächter, K. Segmental Order in Endlinked Polymer Networks: A Monte Carlo Study. *Eur. Phys. J. E* **2005**, *18*, 167−182.
(33) Lipari, G.; Szabo, A. Model-Free Approach to the Interpretation of Nuclear Magnetic Resonance Relaxation in Macromolecules. 1. Theory and Range of Validity. *J. Am. Chem. Soc.* **1982**, *104*, 4546−4559.
(34) Kimmich, R.; Fatkullin, N. Polymer chain dynamics and NMR. *Adv. Polym. Sci.* **2004**, *170*, 1−113.
(35) Brinkmann, A. Edén, M.; Levitt, M. H. Synchronous helical pulse sequences in magic-angle spinning nuclear magnetic resonance: Double-quantum recoupling of multiple-spin systems. *J. Chem. Phys.* **2000**, *112*, 8539−8554.
(36) Sotta, P.; Deloche, B. Long-time dynamics in poly(dimethylsiloxane) networks studied by deuterium nuclear magnetic resonance. *J. Chem. Phys.* **1994**, *100*, 4591−4600.
(37) Williams, M. L.; Landel, R. F.; Ferry, J. D. The Temperature Dependence of Relaxation Mechanisms in Amorphous Polymers and Other Glass-Forming Liquids. *J. Am. Chem. Soc.* **1955**, *77*, 3701−3707.
(38) Doi, M.; Edwards, S. F. *The Theory of Polymer Dynamics*; Clarendon Press: Oxford, 1986.
(39) Demco, D. E.; Hafner, S.; Fülber, C.; Graf, R.; Spiess, H. W. Two-dimensional proton magnetization-exchange NMR spectroscopy in cross-linked elastomers. *J. Chem. Phys.* **1996**, *105*, 11285−11296.
(40) Dollase, T.; Graf, R.; Heuer, A.; Spiess, H. W. Local Order and Chain Dynamics in Molten Polymer-Blocks Revealed by Proton Double-Quantum NMR. *Macromolecules* **2001**, *34*, 298−309.

MA052567B